

to 3000 km wide separated regularly by ~6800 km alongside a dark belt at 50°S that probably pertained to a wave phenomenon resulting from the disturbance. The morphological evolution of this disturbance resembled, on a smaller scale, previous GWS disturbances (5), and it was probably a transient convective phenomenon rapidly dispersed by the zonal winds.

This observation, together with other transient spots observed in recent times (10), suggests that mid-scale storms on Saturn could be more frequent than previously thought. Their detection is a question of the temporal coverage of the observations, the techniques used, and the contrast of the features against the background of normal clouds.

REFERENCES AND NOTES

- A. F. Alexander, *The Planet Saturn* (Faber and Faber, London, 1962).
- A. Sanchez-Lavega, *Icarus* **44**, 1 (1982).
- A. P. Ingersoll, R. F. Beebe, B. J. Conrath, G. E. Hunt, in *Saturn*, T. Gehrels and M. S. Matthews, Eds. (Univ. of Arizona Press, Tucson, 1984), pp. 195–238.
- A. Sanchez-Lavega and E. Battaner, *Astron. Astrophys.* **185**, 315 (1987).
- A. Sanchez-Lavega, *Chaos* **4**, 341 (1994).
- A. Sanchez-Lavega *et al.*, *Nature* **353**, 397 (1991).
- R. F. Beebe, C. D. Barnet, P. V. Sada, A. S. Murrell, *Icarus* **96**, 163 (1992).
- C. D. Barnet, J. A. Westphal, R. F. Beebe, L. F. Huber, *ibid.* **100**, 499 (1992).
- J. A. Westphal *et al.*, *ibid.*, p. 485.
- A. Sanchez-Lavega, J. Lecacheux, F. Colas, P. Laques, *J. Geophys. Res.* **98**, 18857 (1993).
- A. Sanchez-Lavega, J. M. Gomez, J. Lecacheux, F. Colas, I. Miyazaki, *IAU Circ. No. 6079* (1994).
- J. M. Gomez, J. Caquel, P. Laques, *IAU Circ. No. 6059* (1994).
- Most images were taken through filter I (Table 1), which is sensitive to high-altitude hazes. Image processing methods were similar to those described by A. Sanchez-Lavega, J. Lecacheux, F. Colas, and P. Laques [*Science* **260**, 329 (1993)]. For morphology studies, we used an unsharp-mask image processing technique that consists of creating a degraded image from the original one and making an intermediate image from their subtraction. Using some calibration constants, it is possible to obtain a final image that is well contrasted on all parts of the planetary disk up to its edges. This treatment is efficient in discriminating fine features of low contrast.
- Longitudes and zonal wind velocities are measured relative to the System III rotation rate (period = 10 hours and 39.4 min), which is presumed to be that of the planet's magnetic field linked to the planet's interior [M. D. Desch and M. L. Kaiser, *Geophys. Res. Lett.* **8**, 253 (1981)].
- A seasonal radiative-dynamic model of Saturn's troposphere suggests temporal changes in wind speeds within the equatorial region (30°N to 30°S), mainly as a result of ring shadowing and Saturn's tilt [C. D. Barnet, R. F. Beebe, B. J. Conrath, *Icarus* **98**, 94 (1992)].
- These spots could be the manifestation of a planetary Rossby wave. There are at least two well-known examples of waves in Saturn's atmosphere that could be of this type: the polar hexagon [D. A. Godfrey, *Icarus* **76**, 335 (1988)]; M. Allison, D. A. Godfrey, R. F. Beebe, *Science* **247**, 1061 (1990)] and the ribbon wave [L. A. Sromovsky, H. E. Revercomb, R. J. Krauss, V. E. Suomi, *J. Geophys. Res.* **88**, 8650 (1983)]. In its simplest form, the long-wave phase velocity of a Rossby wave can be estimated as $c = -\beta_0 L_R^2$ [G. P. Williams and T. Yamagata, *J. Atmos. Sci.* **41**, 453 (1984)], where $\beta_0 = 2\Omega(\cos \varphi_0)/R$ is the planetary vorticity gradient and $L_R = (gH)^{1/2}/f_0$ is the Rossby deformation radius. Here $\Omega = 1.638 \times 10^{-4}$ rad s⁻¹ is the planetary angular velocity, $\varphi_0 = 9^\circ$ N is the latitude, $R = 60,200$ km is the distance from the center of the planet, g is the acceleration due to gravity, $f_0 = 2\Omega(\sin \varphi_0)$ is the Coriolis parameter, and H is a characteristic vertical scale in the atmosphere. With the above values, $\beta_0 = 5.4 \times 10^{-12}$ m⁻¹ s⁻¹, and c between -100 and -150 m s⁻¹, we get $L_R = 4300$ to 5250 km, corresponding to a wavelength $2\pi L_R = 27,000$ to 33,000 km, comparable with the longitudinal size of WS.
- Standard photometric reduction procedures were applied to the Pic-du-Midi images. Flux calibration in the 300- to 1000-nm spectral region was performed on a beam 2 arc sec in diameter on the center of the disk with the use of recently measured reflectivities [E. Karkoschka and M. G. Tomasko, *Icarus* **106**, 428 (1993); E. Karkoschka, *ibid.* **111**, 174 (1994)]. For the 261-nm filter, we used absolute reflectivity measurements presented by R. A. West *et al.* [*J. Geophys. Res.* **88**, 8679 (1983)]. In the 2000- to 2140-nm spectral range, we used the absolute reflectivities of R. N. Clark and T. B. McCord [*Icarus* **40**, 180 (1979)].
- A. Sanchez-Lavega, J. Lecacheux, F. Colas, P. Laques, *Icarus* **108**, 158 (1994). A Lambert surface of reflectivity A is one that reflects A times the flux incident on it in such a way that the reflected intensity is independent of the direction to the observer.
- The scale height is defined as $H = RT/\mu g$, where R is the gas constant, T is the temperature, and μ is the mean molecular weight of the atmosphere. In Saturn's troposphere, $H \approx 45$ km. The tracers used to measure the Voyager velocities are assumed to have been measured at an average pressure of 400 mbar (20).
- M. G. Tomasko, R. A. West, G. S. Orton, V. G. Tejfel, in *Saturn*, T. Gehrels and M. S. Matthews, Eds. (Univ. of Arizona Press, Tucson, 1984), pp. 150–194; E. Karkoschka and M. G. Tomasko, *Icarus* **97**, 161 (1992).
- There are different observations that suggest that globally the zonal wind velocity decreases with height on Saturn: (i) Atmospheric temperatures at and above the cloud deck (pressure levels of 150, 290, and 730 mbar) derived from Voyager Infrared Interferometer Spectrometer (IRIS) measurements and the thermal-wind relation suggest an averaged vertical wind shear of ~20 m s⁻¹ per scale height [B. J. Conrath and J. A. Pirraglia, *Icarus* **53**, 286 (1983)]. However, an exception was the equatorial region (10° to 25°N), where the eastward equatorial jet increases in speed with height according to this analysis. (ii) On the contrary, HST wind speeds derived from cloud tracking of the equatorial 1990 GWS at two levels (~100 and 300 mbar) gave a zonal wind that decreases by ~45 m s⁻¹ per scale height in the latitude range 0° to 10°N (8), closer to our results.
- The single-scattering albedo ω_0 is the ratio of the particle's cross section for scattering to the sum of its cross sections for scattering and absorption ($\omega_0 = 1$ for purely scattering particles, $\omega_0 = 0$ for absorbing particles). The origin for the short-wavelength absorption is unknown, but an ultraviolet-blue aerosol agent must be mixed with the NH₃ ice particles that presumably form the disturbance clouds.
- E. J. Reese, *Icarus* **15**, 466 (1971).
- We thank R. Beebe for initiating the HST Director's Discretionary Observation of the 1994 Saturn storm as a service to the community, J. R. Acarreta for the radiative-transfer calculations, and two anonymous reviewers for helpful comments. K.N. was a visiting astronomer at the IRTF, operated by the University of Hawaii under contract from NASA. This work was supported by Universidad Pais Vasco (grant EA054/95) and the French National Programme of Planetology.

12 September 1995; accepted 6 December 1995

Group Velocity in Strongly Scattering Media

J. H. Page,* Ping Sheng, H. P. Schriemer, I. Jones, Xiaodun Jing,† D. A. Weitz‡

Investigation of the ballistic propagation of acoustic waves through a resonantly scattering, inhomogeneous medium indicates that although the ballistic signal remains coherent with the incident pulse, it is nevertheless strongly affected by scattering resonances. These resonances cause considerable frequency dispersion and substantially reduce the phase and group velocities. The experimental data are quantitatively described by a theoretical model that correctly accounts for the coupling between the resonant scatterers, leading to an effective renormalization of the scattering within the medium. This approach resolves a long-standing problem in the definition of the group velocity in strongly scattering materials.

Virtually all forms of energy are propagated by waves: heat and sound in the form of acoustic waves, and radio and light in the form of electromagnetic waves. In any medium, wave propagation depends on the relation of the angular frequency of a wave, ω , to its wave vector, k , as given by the dispersion relation $\omega(k)$. Whenever the dispersion relation is nonlinear, waves of different frequencies travel at different speeds and typically require two distinct velocities to describe wave propagation: The first is the phase velocity, $v_p = \omega/k$, the speed at which a plane of constant phase propagates; the second is the group velocity, $v_g = d\omega(k)/dk$, normally the speed at which a

pulse or signal propagates. However, the meaning of the group velocity is strictly well defined only when the dispersion of the medium is not too large (1). Nevertheless, even in a highly dispersive medium, a signal can still propagate, and the determination of its speed of propagation is a classic problem, having been recognized in the work of Sommerfeld (2) and Brillouin (3).

One important manifestation of this problem is the description of wave propagation through strongly scattering, inhomogeneous materials (4). In the intermediate-frequency regime, where the length scale of the inhomogeneities is comparable to the wavelength of the wave, the excitation of

internal modes within the scatterers leads to strong resonant scattering. This scattering results in a large attenuation of the propagating wave, even in the absence of absorption, and a correspondingly large dispersion. The dispersion may lead to unphysical values of the group velocity (5), supporting the ideas of Sommerfeld and Brillouin that the group velocity completely loses its meaning in these circumstances. However, even in the most strongly scattering medium, a coherent, ballistic portion of a transmitted pulse can always be measured if one uses a sufficiently thin sample. This ballistic pulse consists of both the unscattered and forward scattered portions of the wave pulse.

What is the velocity at which this pulse propagates? This question is intriguing because, on the one hand, it does not seem possible for the signal to propagate through the medium without being affected by the scattering, yet on the other hand, if it is scattered, temporal coherence between the transmitted and incident pulses may be destroyed. If the pulse is not scattered, its velocity should be intermediate between the velocities of the individual components of the medium. By contrast, if the scatterers do affect the ballistic propagation, the resultant dispersion may become very large, making the group velocity inadequate to describe ballistic pulse propagation. This question has remained an unresolved dilemma, despite the enormous recent progress in understanding the multiple scattering, diffusion, and possible localization of classical waves (4). In this report, we resolve this basic dilemma.

We focused on ultrasonic waves and measured both the phase and group velocities of the ballistic signals that were transmitted through thin slabs of a strongly scattering material. Strong resonant scattering significantly modified both velocities, making them slower than any of the velocities of the individual components that comprise the medium. We quantitatively calculated both velocities using a generalized effective-medium theory of excitations in the strong scattering limit (6, 7). The same theory also

accurately predicts the measured frequency dependence of the scattering mean free path, establishing a direct link between the dispersion and the excitation of internal resonances within the individual scatterers. The agreement between the theory and experiment provides insight into the origin of the pronounced effects of the strong scattering on the ballistic propagation of sound. It indicates that the coupling between the strong resonant scatterers results in an effective renormalization of the medium through which the ballistic pulse propagates, thereby showing explicitly how coherent wave propagation is influenced by the scattering. The group and phase velocities are significantly reduced but remain well defined and physically meaningful.

The samples were disc-shaped slabs of relatively monodisperse glass beads, randomly packed in water at a glass-bead volume fraction of about 63% and contained between two 1.5-mm-thick sheets of polystyrene. The thickness of the samples ranged from about 2 to 5 mm. Each sample was immersed in water, with a 25-mm-diameter flat transducer generating the sound on one side of the slab and a second, identical receiving transducer on the other side. The frequency of the sound was varied between 1 and 5 MHz, and samples with bead radii of $a = 0.25$ and 0.5 mm were used to increase the effective frequency range. The velocities of ballistic propagation were measured with a square input pulse consisting of about 10 oscillations. Because the detector averages the instantaneous pressure of the acoustic wave over the front face of the transducer, the scattered sound was effectively canceled as a result of its random phase fluctuations in the plane of the detector, reflecting the presence of speckles. This destructive interference left only the unscattered ballistic wave, which was spatially and temporally coherent across the entire surface of the detector. The phase cancellation of the scattered sound was further improved by translating the sample and averaging the transmitted field from different ensembles of the scatterers, thereby ensuring that the background contribution from scattered sound was eliminated from the ballistic pulse.

To determine the phase and group velocities, we used ultrasonic techniques to measure directly the phase and amplitude of the detected signal. The phase velocity was determined from the propagation time of the individual oscillations near the center of the pulse, where the carrier frequency is best defined. The correct correspondence between the oscillations of the incident and transmitted pulses was identified by ensuring consistency of the phase velocity between samples of several different thicknesses. The group velocity was determined

by matching the centers of the transmitted and incident wave forms and measuring the propagation time. We also digitally filtered both the incident and transmitted pulses to limit the signal to a Gaussian pulse with a relatively narrow bandwidth and determined the propagation time of the peak of the pulse. This improved the accuracy of the measurement; however, both techniques yielded essentially the same results.

Significant dispersion was observed (Fig. 1), with the phase velocity dropping by about 50% to a minimum value of 1.25 km/s at $k_w a \approx 3$ (k_w is the acoustic wave vector in water), and with the group velocity varying by about a factor of 2, from a minimum of 0.85 km/s near $k_w a \approx 2$ to a maximum of 1.7 km/s near $k_w a \approx 4.5$. Remarkably, for most of the frequencies at which these measurements were made, both velocities are substantially less than the speed of sound in either of the constituent materials, that is, either the longitudinal velocity in water ($v_w = 1.5$ km/s) or the longitudinal ($v_L = 5.6$ km/s) or transverse velocity ($v_T = 3.4$ km/s) in the glass. Moreover, they are also less than the velocity of interfacial Stoneley waves (8) propagating on a flat interface between glass and water ($v_S \approx 1.5$ km/s).

To calculate these velocities theoretically, we adopted a technique that has been used to determine the dispersion curves for sound propagation through suspensions of solid plastic spheres (6, 7, 9). We begin with the scalar wave equation

$$\left(\nabla^2 + \frac{\omega^2}{v_0^2}\right)\phi + \omega^2[v^{-2}(\mathbf{r}) - v_0^{-2}]\phi = 0 \quad (1)$$

where ϕ denotes the wave amplitude, and $v(\mathbf{r})$ is the local phase velocity, defined by the material parameters at position \mathbf{r} . In the

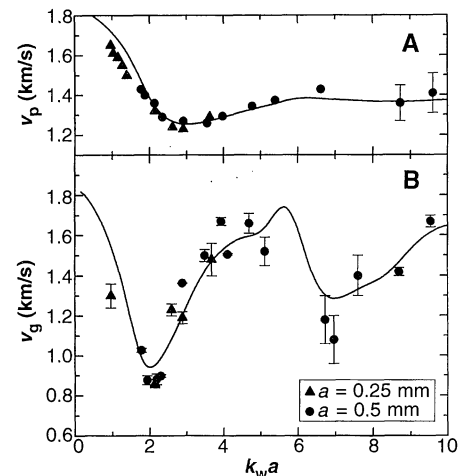


Fig. 1. (A) Phase and (B) group velocities of acoustic waves in a strongly scattering medium consisting of glass beads in water. The data (symbols) are compared with the predictions of the effective medium theory (lines).

J. H. Page, H. P. Schriemer, I. Jones, Department of Physics, University of Manitoba, Winnipeg, MB, Canada R3T 2N2.

P. Sheng, Department of Physics, Hong Kong University of Science and Technology, Clear Water Bay, Kowloon, Hong Kong, and Exxon Research and Engineering, Annandale, NJ 08801, USA.

X. Jing, Department of Chemical Engineering and Materials Science, University of Minnesota, Minneapolis, MN 55455, USA.

D. A. Weitz, Exxon Research and Engineering, Annandale, NJ 08801, USA.

*To whom correspondence should be addressed.

†Present address: Exxon Production Research, P.O. Box 2189, Houston, TX 77252-2189, USA.

‡Present address: Department of Physics, University of Pennsylvania, Philadelphia, PA 19104, USA.

frequency and wave vector representation, the Green's function for Eq. 1, in which the scattering is defined relative to a uniform reference medium with velocity v_0 , is given by

$$G(\omega, k) = \frac{1}{\frac{\omega^2}{v_0^2} - k^2 - \Sigma_{\omega/k}} \quad (2)$$

where the self-energy $\Sigma_{\omega/k}$ represents all of the effects of multiple scattering caused by the inhomogeneities, given by the term $\omega^2[v^{-2}(\mathbf{r}) - v_0^{-2}]$ in Eq. 1. A general approach for obtaining the dispersion relation of excitations in a medium with strong scattering is based on the spectral function given by the negative imaginary part of the Green's function $-\text{Im } G(\omega, k)$. The zeroes of the denominator of the Green's function give the excitations of the system, and the calculation of $-\text{Im } G(\omega, k)$ is one way of delineating this quantitatively. In the low-frequency regime, where the wavelength is much larger than the scale R of the inhomogeneities, there are true zeroes of the denominator in Eq. 2 to leading order of the small parameter R/λ , where λ is the wavelength. These zeroes are in fact the solution of the coherent-potential approximation (CPA) for the calculation of effective medium wave properties (10). However, in the intermediate frequency regime, there are no longer true zeroes; instead, there are only peaks in the function $-\text{Im } G(\omega, k)$. Thus, the CPA approach, at least in its traditional form, can no longer be applied.

To go beyond this limitation, we calculated the spectral function by exploiting the fact that velocity v_0 enters only as a dummy variable in Eqs. 1 and 2, enabling it to be chosen as a free parameter in the calculations (6, 7, 9): As long as the value of v_0 used in the calculations of $\Sigma_{\omega/k}$ is the same as the value appearing in ω^2/v_0^2 , the Green's function is independent of the choice of v_0 . By letting $v_0 = \omega/k$ at every point in the ωk plane and calculating the corresponding values of $\Sigma_{\omega/k}$, we can calcu-

late the spectral function using

$$-\text{Im } G(\omega, k) = \text{Im} \frac{1}{\Sigma_{\omega/k}} \quad (3)$$

This provides a full two-dimensional picture of the frequency and wave vector dependence of the spectral function. Because $\Sigma_{\omega/k}$ represents the effect of the scattering, Eq. 3 tells us that peaks in the spectral function correspond to minima in the scattering. To accurately calculate the self-energy, one must take into account the strong geometric correlation that exists in our random medium, because it is comprised of spheres dispersed in a fluid. To do this, we modeled a typical scatterer within the medium as a sphere coated by a layer of fluid. The thickness of this coating was determined by the volume fraction of the spheres. This coated sphere is embedded in a homogeneous medium whose wave speed is $v_0 = \omega/k$. The self-energy is then obtained by solving the boundary value problem for a plane wave scattering from the embedded coated sphere (7).

This technique is not restricted to scalar waves; the full elastic wave equation can be used for the solid spheres following the same method. This calculation requires knowledge of the longitudinal and transverse velocities in the solid and the longitudinal velocity in the fluid, as well as the densities of the solid and the fluid and the volume fraction of the solid spheres. Using these known parameters for our sample, we calculated the frequency and wave vector dependence of the spectral function (Fig. 2). For comparison with our experimental data, we used the dispersion curve obtained from the peaks of the spectral function to calculate the phase velocity of the glass-bead suspension from the ratio of frequency to wave vector, averaging over the 10% variation in our bead size. Excellent agreement was obtained (Fig. 1A). We also calculated the group velocity by numerically differentiating the dispersion curve (Fig. 1B) and again obtained excellent quantitative

agreement with our data, capturing the full dispersion in v_g observed experimentally.

Further insight into the origin of the dispersion in the group velocity was obtained by measuring the scattering mean free path l_s (Fig. 3). It was determined from the attenuation of the ballistic pulse using the definition $I(L) = I_0 e^{-L/l_s}$, where $I(L)$ is the transmitted intensity for a sample of thickness L and I_0 is the incident intensity. Independent measurements (11) of the diffusely propagating sound have shown that the absorption length is at least 20 times larger than l_s , confirming that the observed attenuation of the ballistic pulse is the result of scattering, not absorption. The relatively large values of l_s at low $k_w a$ reflect the rapid decrease in scattering as the low-frequency Rayleigh regime is approached. Pronounced dips in l_s occur at $k_w a \approx 2$ and 7; these dips correspond almost exactly to the minima observed in the measured group velocity. The origin of these dips can be determined from a calculation of the total scattering cross section of a coated sphere, which is obtained from the imaginary part of the self-energy by using the optical theorem (4). These calculations are in good agreement with the data (Fig. 3), allowing the dips in l_s to be identified with resonances in the total scattering cross section of a single sphere in the medium. These resonances must also be the origin of the dispersion in v_g .

The most surprising feature of the data is that a pulse propagates through the highly dispersive medium at such slow velocities; thus, the transmitted pulse is strongly affected by the scatterers but nevertheless maintains temporal and spatial coherence with the incident pulse. The agreement of the calculated group velocity with the data suggests a physical picture for this behavior. When the scattering is strong, each scatterer must sense the scattered waves from the other particles. As a result, the embedding medium becomes renormalized, an effect that is analogous to the shifting of two

Fig. 2. Magnitude of the spectral function plotted as a function of normalized frequency $\omega a/v_w$ and wave vector ka . The magnitude is indicated by the colors, with red being high and blue being low (the scale bar is in arbitrary units). The dispersion curve, defined by the peaks, is accurately determined because the widths of the peaks are substantially less than their central frequencies. This dispersion curve (solid white line) falls below the dispersion curve for pure water (dashed line) over most of the frequency range. These calculations involve no adjustable parameters.

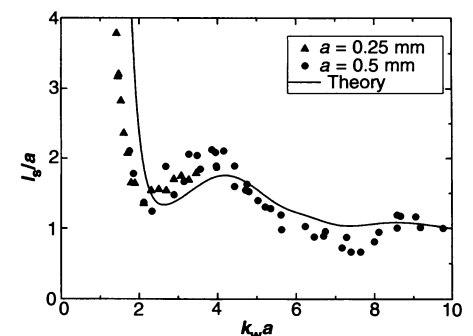
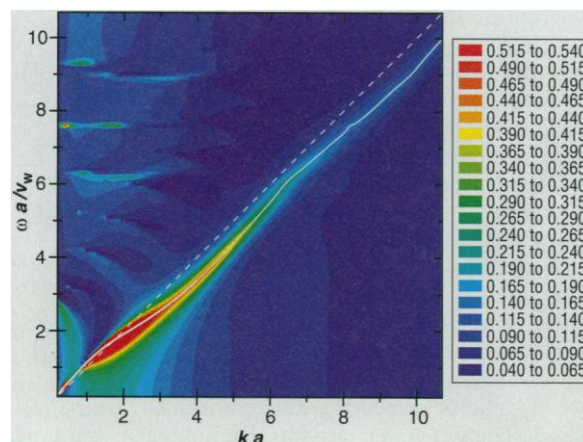


Fig. 3. Scaled scattering mean free path l_s/a as a function of normalized frequency $k_w a$. The curve shows a calculation based on the scattering cross section of a single coated sphere.

quantum mechanical resonances when they are strongly coupled. The amount of this renormalization depends on the strength of scattering; the larger the scattering, the larger the adjustment. Moreover, it is physically plausible that as the concentration of scatterers increases, the material properties of the renormalized effective embedding medium approach those of the scatterers themselves. Consequently, the individual scattering resonances inevitably become leaky and weakened, as the effective contrast between a scatterer and the embedding medium diminishes. In fact, in the limit of the embedding medium having the same properties as the scatterers, the resonances must vanish entirely. It is precisely this effective renormalization of a strongly scattering medium that is sensed by the coherent group velocity. In our calculation, the coated sphere also possesses these scattering resonances, and these are modified by the coupling to the embedding medium. Our procedure effectively identifies the frequencies and wave vectors of the minima in these coupled scattering resonances; these correspond to the dispersion curve. This approach indicates directly how a propagating wave of frequency ω is forced by the renormalization of the embedding medium to select the wave vector k that allows it to propagate through the medium with the least scattering. Hence, the physical origin of the remarkably low velocities of ballistic propagation lies in the renormalization of the effective medium by strong resonant scattering, as correctly described by our theoretical model. Finally we note that, although our experimental and theoretical approach has focused on acoustic waves, we expect the same features to be observed for any form of classical wave propagating in disordered materials; thus, electromagnetic radiation, such as light or microwaves, should show similar behavior, and confirmation of this would provide an important generalization of our results.

REFERENCES AND NOTES

1. J. D. Jackson, *Classical Electrodynamics* (Wiley, New York, ed. 2, 1975).
2. A. Sommerfeld, *Ann. Phys. (Leipzig)* **44**, 177 (1914).
3. L. Brillouin, *Wave Propagation in Periodic Structures* (Dover, New York, 1953); *Wave Propagation and Group Velocity* (Academic Press, New York, 1960).
4. P. Sheng, *Introduction to Wave Scattering, Localization and Mesoscopic Phenomena* (Academic Press, New York, 1995).
5. M. P. van Albada, B. A. van Tiggelen, A. Lagendijk, A. Tip, *Phys. Rev. Lett.* **66**, 3132 (1991).
6. X. D. Jing, P. Sheng, M. Y. Zhou, *ibid.*, p. 1240.
7. ———, *Phys. Rev. A* **46**, 6513 (1992).
8. L. M. Brekhovskikh, *Waves in Layered Media* (Academic Press, New York, 1980).
9. P. Sheng, X. Jing, M. Zhou, *Physica A* **207**, 37 (1994).
10. E. N. Economou, *Green's Functions in Quantum*

Physics (Springer-Verlag, Berlin, 1979).

11. J. H. Page, H. P. Schriemer, A. E. Bailey, D. A. Weitz, *Phys. Rev. E* **52**, 3106 (1995).
12. We thank K. S. Beatty and M. L. Cowan for their assistance, and the Natural Sciences and Engineer-

ing Research Council of Canada and the North Atlantic Treaty Organization for their support of this project.

1 September 1995; accepted 7 December 1995

Calcification in Hermatypic and Ahermatypic Corals

A. T. Marshall

The evolutionary development of tropical coral reefs is presently ascribed to the association of corals with symbiotic algae (zooxanthellae) and to the enhancement of calcification by light. Contrary to this idea, the calcification rate in a non-reef-building tropical coral (*Tubastrea faulkneri*) without symbiotic algae was the same as the light-enhanced rate in a zooxanthellate reef-building coral (*Galaxea fascicularis*). The mechanisms of calcification, however, differed between the two species. Instead of being "light-enhanced," calcification in corals with algae was "dark-repressed." The evolutionary development of coral reefs may therefore not be related to light-enhanced calcification resulting from the association of corals with symbiotic algae.

It is generally thought that the formation of coral reefs in shallow tropical seas has been possible because the association of symbiotic algae (zooxanthellae) with hermatypic (reef-building) corals facilitates rapid calcification. The calcification rate of zooxanthellate hermatypic corals has been considered to be greater than that of azooxanthellate corals [categorization according to Schuhmacher and Zibrowius (1)]. Calcification in the former is said to be light-enhanced (2). It is indisputable that light profoundly affects calcification rates in these corals, the phenomenon first being noted by Kawaguti and Sakumoto (3) and subsequently confirmed by Goreau (4) and many other authors (2). The experimental evidence, however, supporting the assertion that calcification in zooxanthellate hermatypic corals proceeds at a higher rate than in azooxanthellate corals appears to be very limited. The evidence is largely based on the finding that the calcification rate in an ahermatypic Atlantic coral *Astrangea danae* was so low at 8° to 10°C as to be undetectable (5). Although *Astrangea* is an ahermatypic coral, it appears to have a facultative symbiotic relation with zooxanthellae. Jacques *et al.* (6) showed that colonies of *Astrangea* that contained zooxanthellae did exhibit light-enhanced calcification at 15° to 27°C, with calcium incorporation rates that were comparable to those of reef corals. These experiments do not show that tropical azooxanthellate corals, which never contain zooxanthellae, calcify at lower rates than do tropical zooxanthellate hermatypic corals. The supposition that the calcification rate is lower in tropical azooxanthellate corals then rests primarily on observations

showing that rates are lower in hermatypic corals that have been experimentally deprived of zooxanthellae (4); there appear to be no measurements of calcification rates in tropical azooxanthellate corals and therefore no direct comparisons. The present paper seeks to rectify this omission.

Experiments were carried out at Heron Island Research Station on the Great Barrier Reef of Australia. Two species of coral were selected that have large discrete polyps that can be readily separated. The hermatypic zooxanthellate coral *Galaxea fascicularis* has polyps of similar size and form to those of the ahermatypic azooxanthellate coral *Tubastrea faulkneri*, and care was taken to use polyps from the same colonies and match the sizes of polyps from each species as closely as possible.

Two experiments designed to measure ⁴⁵Ca incorporation into the coral skeleton were carried out on different days. Polyps were incubated in containers of aerated filtered seawater placed in large outdoor aquariums under the same conditions of time (4 hours) and temperature (25°C) (7). *Tubastrea* was incubated in shade (5 μmol s⁻¹ m⁻²) because it is normally found subtidally on coral reefs in caves or under overhangs. *Galaxea* was obtained intertidally and was incubated in full sunlight (540 to 1080 μmol s⁻¹ m⁻²). The rates of calcium incorporation per mass of skeleton (8) were shown to be the same in the two species, being 0.65 ± 0.18 μmol g⁻¹ hour⁻¹ (n = 5) for *Tubastrea* and 0.60 ± 0.09 μmol g⁻¹ hour⁻¹ (n = 5) for *Galaxea* (P > 0.05, t test).

A further experiment was carried out under similar conditions but for a longer period of time (6.5 hours) and at higher temperature (27° to 28°C). Polyps of *Tubastrea* and *Galaxea* were incubated in ⁴⁵Ca

Analytical Electron Microscopy Laboratory, School of Zoology, LaTrobe University, Bundoora (Melbourne), Victoria 3083, Australia.